A model of the prolate chromosphere formation at the solar minimum(*)

B. P. Filippov(1), S. Koutchmy(2) and O. G. Den(1)

(1) *Institute of Terrestrial Magnetism, Ionosphere and Radio Wave Propagation*
    Russian Academy of Sciences - Troitsk Moscow Region, 142190, Russia
(2) *Institut d'Astrophysique de Paris, CNRS - 98 bis Boulevard Arago, F-75014 Paris, France*

Summary. — Detailed observations in different chromospheric lines of a solar diameter in polar and equatorial directions showed that the polar chromosphere at the minimum phase of solar cycle looks more extended than the low-latitude chromosphere. We propose a simple geometric model to explain the effect of the prolateness of the solar chromosphere. A specific dynamical part of the solar atmosphere above the 2 Mm level is assumed to be a mixture of moving up and down jets of chromospheric matter with the coronal plasma between them. Due to the dynamic nature of this layer, the magnetic field is considered to play a very important role in the density distribution with the height, guiding the mass flows along the field lines. The difference of the magnetic-field topology in the polar and the equatorial regions leads to different heights of the chromospheric limb.

PACS 95.30.Qd – Magnetohydrodynamics and plasmas.
PACS 96.60.-j – Solar physics.
PACS 01.30.Cc – Conference proceedings.

1. – Introduction

In contrast to the solar white-light limb looking like a perfect circle, polar chromosphere at the minimum of activity looks more extended than the low-latitude chromosphere [1-4]. The prolateness is up to 1.5 Mm being different in the different chromospheric spectral lines (table I). This fact was in particular found in ground-based observations at Arcetri Observatory in the '40s and was confirmed recently in space-based observations with SOHO EIT.

The upper part of the chromosphere is far from the static state. It consists of numerous thin jet-like structures filling magnetic flux tubes. High-resolution images of the solar

TABLE I. – *Heights of the average limb positions taken above the level $h_{\tau_5=1} + 2$ Mm as observed using different chromospheric spectral lines.*

Element	Line	Height of the dynamical chromosphere at poles (Mm)	Height of the dynamical chromosphere at equator (Mm)	Prolateness over a solar radius (Mm)	Model estimation of the height of dynamical chromosphere; at equator (Mm)
H	Hα	3.3 ± 0.35	2.2 ± 0.35	1.1 ± 0.35	2.8
Ca II	K2	0.85 ± 0.1	0.65 ± 0.1	0.2 ± 0.1	0.81
Ca II	K3	1.8 ± 0.15	1.35 ± 0.15	0.45 ± 0.15	1.65
He II	30.4 nm	4.5 ± 0.5	3.0 ± 0.5	1.5 ± 0.5	3.68
He I	1083 nm	0 ± 0.3	0 ± 0.3	0 ± 0.3	0
	D₃	0 ± 0.3	0 ± 0.3	0 ± 0.3	0

limb in Hα shows a "forest" of spike-like features. The highest of them are more straight and tilted to the vertical within the angle of 20–30°. In the lower part one can see a number of arches. We assume that the dynamical part of the solar atmosphere, being a mixture of moving up and down jets of chromospheric matter and coronal plasma between them, is responsible for the solar prolateness. Due to the dynamic nature of this layer, the magnetic field plays a very important role in the density distribution with respect to the height, guiding the mass flows along the field lines. In this paper we attempt to calculate the magnetic field on the base of direct measurements of the field in the photosphere and find out the difference in the magnetic field scales in the equtorial and polar regions.

2. – Description of the model

We assume that network magnetic elements in polar regions are predominantly of the same polarity. In the quiet solar equatorial regions, they are of mixed polarity (fig. 1). For ballistic jet motion (which is not exact for a large part of spicules but can be assumed as a first approximation), the maximum height of a spicule would be the same for all trajectories along the curved field lines if a line reaches this height. In the polar region all jets are able to ascend up to a gravitationally limited height. The mean density distribution in the upper polar chromosphere is determined by i) the scale height in an individual spicule and ii) the distribution of the number of spicules *vs.* the height. In the equatorial region some jets will be forced to come down after they reach the apex of a relatively low arch. When considering the average over time heights reached by spicules,

Fig. 1. – Schematic representation of the magnetic-field lines and plasma jets at the pole (left) and at the equator (right).

this factor will reduce the mean chromosphere density at a given height proportionally to the fall of the magnetic flux of one polarity:

$$(1) \qquad \rho(z) = \rho_0 \left(\frac{\Phi(z)}{\Phi_0} \right) e^{-z/h} \,,$$

where h is the *effective* scale height which is considerably larger than the 0.2 Mm hydrostatic scale height. In the previous paper [5] we modelled the network magnetic-field concentrations as "magnetic charges" which arranged in the equatorial region with alternating signs. If we choose the mean separation between opposite polarity concentrations to be about 9 Mm, we obtain the prolateness which is within the uncertainties of the measurements in all spectral lines. The distance 9 Mm seems to be reasonable because it is independently revealed by other processes in the chromosphere and it may even be found directly in the magnetic-field pattern coming from the most typical magnetograms of the quiet Sun.

Contrary to the schematic model outlined in [5], magnetic-field calculations show that the magnetic flux decreases with height both in the equatorial region and in the polar region. In fact, the situation is intermediate between the cases shown in the left-hand and right-hand parts of fig. 1. The net magnetic flux through a given region of the photosphere is both non-zero and not of one polarity. Although we may expect the fall of the flux in the polar region to be slower.

We can introduce the scale height b for the magnetic flux

$$(2) \qquad \left(\frac{\Phi(z)}{\Phi_0} \right) = e^{-z/b} \,,$$

that can be found from the magnetic-field calculations

$$(3) \qquad b = -\frac{\Phi}{\partial \Phi/\partial z} \,.$$

If we assume that the density at the top of the chromosphere is a factor e^k less than the density at the base, then we obtain

$$(4) \qquad e^{-k} = e^{-z/b} \, e^{-z/h} \,,$$

or

$$(5) \qquad k = z \left(\frac{1}{b} + \frac{1}{h} \right) \,.$$

Applying this relationship to the polar and equatorial regions we can exclude the unknown *effective* scale height h and express the height of the dynamical equatorial chromosphere z_e in terms of the scale height b_p for the magnetic flux in the polar region, b_e in the equatorial region, and the height of the dynamical polar chromosphere z_p

$$(6) \qquad z_e = \frac{kb_p b_e z_p}{kb_p b_e + z_p(b_p - b_e)} \,.$$

3. – Magnetic-field calculations

The coronal magnetic field is usually calculated by extrapolating the field from the photospheric level. The potential magnetic field in the corona can be found by solving the Neumann external boundary-value problem. There are a number of methods to solve this problem numerically [6-8]. The first code was developed and successfully used by Schmidt [9]. Since we are concerned with the magnetic field in the chromosphere and low corona, at a height which is small compared with the solar radius, we may neglect sphericity and use the well-known solution for half-space with a plane boundary (see, *e.g.*, [10]).

$$
\mathbf{B} = \frac{1}{2\pi} \int \int_S \frac{B_n(x', y', 0)\,\mathbf{r}}{r^3}\,\mathrm{d}x'\mathrm{d}y', \tag{7}
$$

where $B_n(x', y', 0)$ is the normal magnetic-field component in the plane S and $\mathbf{r}$ is the radius vector from a point in the surface to a given point in the corona. The integration can be performed analytically within a small rectangular area with the constant value of $B_n(x', y', 0)$ [11]. This area represents a unit of the spatial resolution of a magnetograph.

The above algorithm can be easily used in the equatorial region for an area located not far from the central meridian. The measured line-of-sight field component represents here the normal component with sufficient accuracy. In the polar region, the normal direction differs significantly from the line of sight. So we were forced to use a specific method to calculate the field at the base of the boundary condition with the "tilted" component B_l. One method was proposed by Semel [12]. It is based on the solution of Dirichlet problem for B_l component. A different method described first in [11] uses the solution of an integral equation.

We define Cartesian coordinates with the z-axis normal to the boundary plane $z = 0$ (*i.e.* the photosphere). The magnetic-field component along the direction $\mathbf{l}$ is

$$
B_l = B_x\cos\alpha + B_y\cos\beta + B_z\cos\gamma, \tag{8}
$$

where α, β, γ are the angles between the $\mathbf{l}$ direction and the coordinate axes x, y, z. The normal component $B_n = B_z$ in the boundary plane is expressed as

$$
B_n(x, y, 0) = B_l(x, y, 0)\frac{1}{\cos\gamma} - B_x(x, y0)\frac{\cos\alpha}{\cos\gamma} - B_y(x, y, 0)\frac{\cos\beta}{\cos\gamma}, \tag{9}
$$

where $B_x(x, y, 0)$ and $B_y(x, y, 0)$ are the field components defined by (7). These expressions have singularities in the boundary plane which are eliminated after analytical integration within small rectangular areas with the constant value of $B_n(x, y, 0)$ [11]. Let for simplicity the y-axis be perpendicular to the direction $\mathbf{l}$. Then $\cos\beta = 0$ and $\cos\alpha = \sin\gamma$. Substituting the expression for B_x from eq. (7) into (9), we find

$$
B_n(x, y, 0) = B_l(x, y, 0)\frac{1}{\cos\gamma} - \tan\gamma\frac{1}{2\pi} \int \int_S \frac{B_n(x', y', 0)\,(x - x')}{r^3}\,\mathrm{d}x'\mathrm{d}y'. \tag{10}
$$

Equation (10) is an integral equation with respect to B_n. We can solve it by iterations consequently substituting the right-hand part of eq. (10) into the integral. Let us
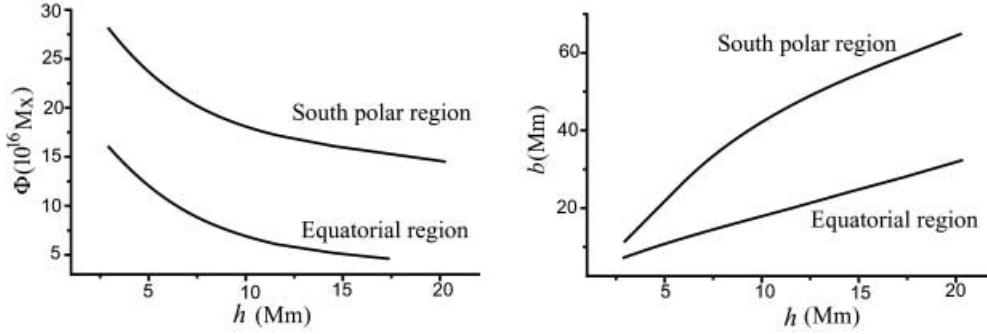
Fig. 2. – The dependence of the southern polarity magnetic flux Φ (left) and the scale height b for the magnetic flux (right) on the height h above the photosphere at the pole and at the equator.

introduce the following designation:

$$(11) \qquad [x|\varphi|x'] = \frac{1}{2\pi} \int\!\!\int_S \frac{\varphi(x',y',0)\,(x-x')}{r^3}\,\mathrm{d}x'\mathrm{d}y'\,.$$

According to this notation eq. (10) can be rewritten as

$$B_n(x,y,0)\,\cos\gamma = B_l(x,y,0) - \tan\gamma\,[x|B_l|x'] + \tan^2\gamma[x[x'|B_l|x'']x'] -$$
$$-\tan^3\gamma\,[x[x'[x''|B_l|x''']x'']x'] + ...$$
$$+(-1)^n\tan^n\gamma\,[x[x'...[x^{(n-1)}|B_l|x^{(n)}]...x'']x'] +$$
$$+(-1)^{n+1}\tan^n\gamma\,\sin\gamma\,[x[x'...[x^{(n)}|B_n|x^{(n+1)}]...x'']x'],$$

where $x', x'', ..., x^{(n)}$ are the variables of the integration.

Thus, the normal component is expressed as an infinite series with the terms of different signs. Parameter $\tan\gamma$ provides the convergence of the series, so $\tan\gamma < 1$ or $\gamma < 45°$. This factor defines the number of the series terms needed to obtain the necessary precision. When the angle between $\mathbf{l}$ and $\mathbf{n}$ is greater than $45°$ another modification of the method is used. The role of the small factor is played here by $\sin\gamma$ [13].

4. – Results and discussion

We used magnetograms obtained with Michelson Doppler Imager (MDI) onboard SOHO, which are accessible at `http://sohodb.nascom.nasa.gov/summary/`. The measurements within areas close to the limb have rather low precision and a noise level is several times greater than a noise level near the center of the disk. For these reasons the calculated magnetic field above a domain at the disk center differs significantly from the field calculated above the same area near the east or west limb. Since the polar region can be observed only near the limb, we compare the polar magnetic field with the field above a domain in the equatorial region near the limb too in order to have more uniform boundary data. Figure 2 shows the dependence of the negative magnetic flux through the area of a domain on the height for two domains centered about $65°$ from the center of the solar disk in the South polar and West limb equatorial regions on October 24, 1998.

TABLE II. – *The scale height b for the magnetic flux in the polar and the equatorial regions.*

Data	23.08.1996	02.11.1996	22.04.1997	23.06.1998	24.10.1998
$b_{\rm p}$ (Mm)	6.24	6.89	10.5	6.31	11.2
$b_{\rm e}$ (Mm)	7.00	5.63	7.32	6.24	7.24

The right-hand part of fig. 2 shows the dependence of the magnetic flux scale height in the two regions. We chose the dominant southern polarity because it is the dominant polarity in the domain that guides the most of mass flows in the region. Substituting $b_{\rm p} = 11.2$ Mm and $b_{\rm e} = 7.24$ Mm into formula (6) we find the height of the equatorial chromosphere. Calculated values are presented in the last column of table I. They seem to be rather close to the observed heights although they are not exactly within error bars of the observations. However, the coincidence is worse for other four days we analyzed. The scale heights are presented in table II. It is seen that the difference in the polar and equatorial scale heights is less than on October, 24, 1998. Moreover, the relationship between them is opposite on August 23, 1996. Unfortunately, magnetic data during the period of prolateness measurements on August 1998 are not available because at this time SOHO was out of control. Since the effect of prolateness is statistical and table I presents the average values, we could assume that more statistics is needed to check the model. However, we feel that the MDI magnetic-field data in the regions so close to the limb are too inaccurate and noisy for our purpose. We think that more accurate polar magnetic-field measurements could shed light on this problem.

$$* \; * \; *$$

REFERENCES

[1] SECCHI S. J., *Le Soleil* (Gauthier-Villars) 1877, p. 38.
[2] FRACASTORO M. G., *Pub. R. Oss. Arcetri*, **64** (1948) 44.
[3] JOHANNESSON A. and ZIRIN H., *Astrophys. J.*, **471** (1966) 510.
[4] AUCHERE F., BOULADE S., KOUTCHMY S., SMARTT R. N., DELABOUDINIERE J. P., GEORGAKILAS A., GURMAN J. B. and ARTZNER G. E.,*Astron. Astrophys.*, **366** (1998) L57.
[5] FILIPPOV B. and KOUTCHMY S., *Solar Phys.*, **196** (2000) 311.
[6] ALTSCHULER M. D. and NEWKIRK G., *Solar Phys.*, **9** (1969) 131.
[7] LEVINE R. H., *Solar Phys.*, **44** (1975) 365.
[8] ADAMS J. and PNEUMAN G. W., *Solar Phys.*, **46** (1976) 185.
[9] SCHMIDT H. U., in *AAS-NASA Symposium on Physics of Solar Flares*, edited by W. HESS (NASA Spec. Publ. SP-50), 1964, pp. 107.
[10] TIKHONOV A. N. and SAMARSKII A. A., *Equations of Mathematical Physics* (Nauka, Moscow) 1972, p. 363.
[11] DEN O. G., DEN O. E., KORNITSKAYA E. A. and MOLODENSKII M. M., *Soln. Dannye*, **1** (1979) 97.
[12] SEMEL M., *Ann. Astrophys.*, **30** (1967) 513.
[13] DEN O. G., *Astron. Lett.*, **28** (2002) 345.